UVicSPACE: Research & Learning Repository

University of Victoria

Faculty of Science

Faculty Publications

Light trapping in a-Si:H thin solar cells using silver nanostructures

P. H. Wang, M. Theuring, M. Vehse, V. Steenhoff, C. Agert, and A. G. Brolo

January 2017

© 2017 Wang et al. This is an open access article distributed under the terms of the Creative Commons Attribution License. http://creativecommons.org/licenses/by/4.0

This article was originally published at:

https://doi.org/10.1063/1.4973987

Citation for this paper:

Wang, P. H.; Theuring, M.; Vehse, M.; Steenhoff, V.; Agert, C.; & Brolo, A. G. (2017). Light trapping in a-Si:H thin solar cells using silver nanostructures. *AIP Advances*, 7(1).

Light trapping in a-Si:H thin film solar cells using silver nanostructures

P. H. Wang, M. Theuring, M. Vehse, V. Steenhoff, C. Agert, and A. G. Brolo

Citation: AIP Advances **7**, 015019 (2017); doi: 10.1063/1.4973987
View online: https://doi.org/10.1063/1.4973987
View Table of Contents: http://aip.scitation.org/toc/adv/7/1
Published by the American Institute of Physics

Articles you may be interested in

On the propagation of electromagnetic waves in isotropic media that are both electrically and magnetically dispersive
AIP Advances **7**, 015018 (2017); 10.1063/1.4973869

Surface plasmon enhanced silicon solar cells
Journal of Applied Physics **101**, 093105 (2007); 10.1063/1.2734885

Tunable light trapping for solar cells using localized surface plasmons
Journal of Applied Physics **105**, 114310 (2009); 10.1063/1.3140609

Design principles for particle plasmon enhanced solar cells
Applied Physics Letters **93**, 191113 (2008); 10.1063/1.3021072

Plasmonic nanoparticle enhanced light absorption in GaAs solar cells
Applied Physics Letters **93**, 121904 (2008); 10.1063/1.2988288

Detailed Balance Limit of Efficiency of p-n Junction Solar Cells
Journal of Applied Physics **32**, 510 (1961); 10.1063/1.1736034

Light trapping in a-Si:H thin film solar cells using silver nanostructures

P. H. Wang,[1] M. Theuring,[2,a] M. Vehse,[2] V. Steenhoff,[2] C. Agert,[2] and A. G. Brolo[1,b]
[1]*Department of Chemistry, University of Victoria, Victoria BC V8W 3V6, Canada*
[2]*NEXT ENERGY, EWE Research Centre for Energy Technology, University of Oldenburg, 26129 Oldenburg, Germany*

(Received 20 October 2016; accepted 30 December 2016; published online 10 January 2017)

Plasmonic thin film solar cells (modified with metallic nanostructures) often display enhanced light absorption due to surface plasmon resonance (SPR). However, the plasmonic field localization may not be significantly beneficial to improved photocurrent conversion efficiency for all types of cell configurations. For instance, the integration of random metallic nanoparticles (NPs) into thin film solar cells often introduces additional texturing. This texturing might also contribute to enhanced photon-current efficiency. An experimental systematic investigation to decouple both the plasmonic and the texturing contributions is hard to realize for cells modified with randomly deposited metallic nanoparticles. This work presents an experimental and computational investigation of well-defined plasmonic (Ag) nanoparticles, fabricated by nanosphere lithography, integrated to the back contact of hydrogenated amorphous silicon (a-Si:H) solar cells. The size, shape, periodicity and the vertical position of the Ag nanoparticles were well-controlled. The experimental results suggested that a-Si:H solar cells modified with a periodic arrangement of Ag NPs (700 nm periodicity) fabricated just at the top of the metal contact in the back reflector yields the highest improvement in terms of current density (J_{SC}). Finite-difference time-domain (FDTD) simulations also indicated that Ag nanoparticles located at the top of the metal contact in the back reflector is expected to lead to the most efficient light confinement inside the a-Si:H absorber intrinsic layer (i-layer). *© 2017 Author(s). All article content, except where otherwise noted, is licensed under a Creative Commons Attribution (CC BY) license (http://creativecommons.org/licenses/by/4.0/).* [http://dx.doi.org/10.1063/1.4973987]

Designs for low-cost and large area nanostructured solar cells that present enhanced photoconversion have been widely demonstrated.[1,2] In most cases, the introduction of nanostructures improves light trapping, which is crucial to enhance power conversion efficiency (PCE) in thin film solar cells.[3–7] Plasmonic nanostructures (metallic nanostructures that support surface plasmon excitations) exhibit one of the largest extinction cross sections. This effect has been shown to improve light trapping in several thin film solar cells architectures.[7–10] For instance, metallic nanoparticles (NPs) embedded in thin film solar cells act as antennas that capture the incident light and store its energy in localized surface plasmon resonance (LSPR) modes. This energy can either be transferred to the semiconductor layer by near-field coupling or scattered by the NPs towards the active material.[4,5,9–12] Previous works have demonstrated photocurrent enhancement for metallic NPs embedded in several types of thin-film cells, including organic solar cells,[13,14] CdTe-based solar cells[15] and silicon solar cells.[16,17] Improved external quantum efficiency (EQE) in hydrogenated amorphous silicon (a-Si:H) thin film solar cells have been demonstrated by introducing random silver (Ag) NPs in the solar design.[3,16,18] Although enhanced photocurrent relative to a reference without any nanostructures was

[a]This research was performed while M. Theuring was at NEXT ENERGY, EWE Research Centre for Energy Technology, University of Oldenburg, 26129 Oldenburg, Germany.
[b]Author to whom correspondence should be addressed. Electronic mail: agbrolo@uvic.ca.

 © Author(s) 2017

observed, it was not possible to definitely assign the observed enhanced photocurrent to a plasmonic effect. This is because the observed photocurrent improvement could to a significant extent stem from other factors, such as increased surface roughness. Surface roughness (or texturing) is known to affect both the magnitude and the maximum absorption wavelength of a photovoltaic device.[5,11] A way to possibly de-convolute plasmonic effects from texturing contributions is to integrate well-organized metallic nanostructures in solar cells, since they should present much more defined optical characteristics. Several groups have conducted experimental measurements and computational calculations with organized nanostructures integrated in thin film solar cells. The focus of those works was on the relationship between the enhanced photocurrent and the spectral response of the organized arrangement of nanostructures.[4,17,19] Although those previous investigations contributed significantly to our understanding of how both optical and electrical properties need to be optimized to improve PCE in a thin film a-Si:H device, a systematic investigation of the different light trapping contributions is still lacking. On the other hand, insights into the relative influence of the various light trapping contributions can be inferred from a systematic investigation of the solar cell design. By varying the geometric characteristics, such as size, position and periodicity, of a thin film solar cell back reflector (BR) modified with organized metallic (plasmonic) nanostructures, a more complete picture of the different contributions can be obtained.

In this work, a-Si:H thin film solar cells modified with well-organized arrangements of metallic NPs fabricated by nanosphere lithography (NSL) were investigated. Both experimental results and finite-difference time-domain (FDTD) simulations suggested that the geometry of the cell structure and the position of the nanoparticles within the BR have a higher influence on light trapping properties than the near-field plasmonic contribution for thin film silicon solar cells.

Fig. 1 presents a schematic of a thin-film silicon solar cell modified with Ag NPs fabricated by NSL. Ag NPs were embedded in a ZnO:Al buffer layer, just on top of a Ag film as part of the BR, as indicated in Fig. 1. Note that the total thickness of the ZnO:Al TCO buffer layer was kept constant at 80 nm. This thickness was determined in optimized antireflection coating experiments without the nanostructures. The distance (D) between the Ag mirror and the Ag nanostructures was systematically varied by changing the position of the Ag nanostructure within the ZnO:Al film (D=60, 40, 20 and 0 nm away from the Ag mirror, a schematic of the four nanostructured configurations is also shown in Fig. 1) for each periodicity (P=500, 700, 1000 and 1500 nm) investigated. The optimized height of the Ag NPs was 120 nm, and the Ag was e-beam evaporated in all cells. Solar cells were fabricated on all plasmonic BR substrates in n-i-p configuration (deposition order: n-doped/intrinsic/p-doped) by plasma-enhanced chemical vapor deposition and in a shared process to ensure comparability (see supplementary material (SM) for experiment details). The large area patterning of the BR was achieved using NSL. This technique is very robust and it is known to yield structures with relative low defect densities in a large area.[20] The low level of defects in the organized structures had no significant consequences to the performance of the solar cells.

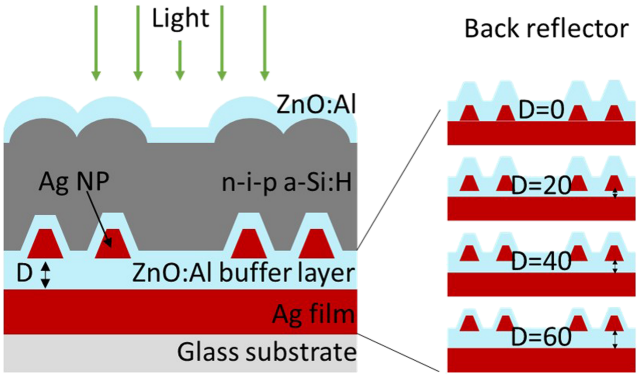

FIG. 1. Schematic of a nanostructured a-Si:H solar cell design: the distance (D) between the Ag film and the Ag nanostructures was systematically varied by changing the position of the Ag nanostructure within the ZnO:Al TCO buffer layer (D=60, 40, 20 and 0 nm away from the Ag film).

Fig. 2a presents a photograph of the different Ag NPs-modified plasmonic BR substrates for 700 nm (left) and 1.0 μm (right) periodicity, respectively. The picture shows a strong color/wavelength dependence on the Ag NPs D-values (D = 60, 40, 20 and 0 nm as indicated in Fig. 2a) for both periodicities. This color/wavelength dependence originates from both diffraction and SPR effects.[2] The Ag NPs modified BR is then expected to affect the overall solar cell performance. Fig. 2b presents a cross section SEM of an a-Si:H n-i-p solar cell fabricated on top of the plasmonic BR. In Fig. 2b, the Ag NPs are hexagonally packed inside an a-Si:H solar cell with 700 nm periodicity and D = 20 nm. Each layer (TCO and a-Si:H n-i-p) grew conformal around the Ag NPs, resulting in a well-organized, dome-shaped, surface. The individual layers are indicated in the inset of the SEM image in Fig. 2b, and the Ag NPs embedded in the BR are labeled in blue color.

The effects of the Ag NPs periodicity and D-values on the performance of the nanostructured solar cells are summarized in Fig. 3. The graph shows the experimental a-Si:H solar cell parameters for D = 60, 40, 20 and 0 nm and for periodicities equal to 500, 700, 1000 and 1500 nm, respectively. All the cells were fabricated in the same batch, in order to minimize batch-to-batch variations. A total of 144 cells were fabricated and characterized, and each point in Fig. 3 is an average of 9 cells. One observes that both, the periodicity of the NPs as well as their position in the ZnO:Al BR have an influence on the solar cell performance. While the open circuit voltage (V_{OC}) varies only slightly around the value of 855 mV, FF increases towards smaller periodicities, from ~55 % (periodicity = 1500 nm) to ~65 % (periodicity = 500 nm). The average PCE of the nanostructured solar cells varied approximately between 5% and 6%, with a maximum PCE close to 6.5% (500 nm periodicity), compared to 4.5% for the flat reference (without Ag NPs). Note that the geometry of Ag NPs and dome-shaped surface for each different periodicity was slightly different, due to the different PS voids. However, the solar cell geometry does not change with varying D values when the periodicity is kept constant. It is important to point out that the relative low efficiency of our devices (~6% in Figure 3, compared to typical ~12% for thin film a-Si:H) does not affect the reliability of the

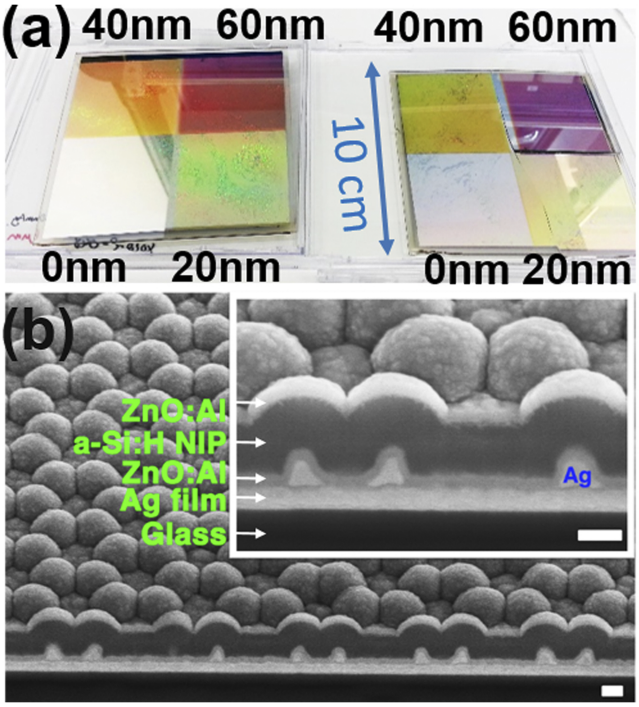

FIG. 2. (a) An optical image of Ag NPs-modified plasmonic back reflector (BR) with different D–values (see Fig.1) indicated in the image; fabricated in a 10 cm x 10 cm scale using NSL. Different periodicities (P = 700 nm (left) and P = 1.0 μm (right)) are shown. (b) A cross section SEM of a Ag NPs-modified (P = 700 nm, D = 20 nm) a-Si:H n-i-p solar cell. The cross section was milled by focused ion beam (FIB); viewed at 45 degrees tilt angle; the cell stacks are indicated in the inset of the SEM image. Scale bars in (b) are 200 nm.

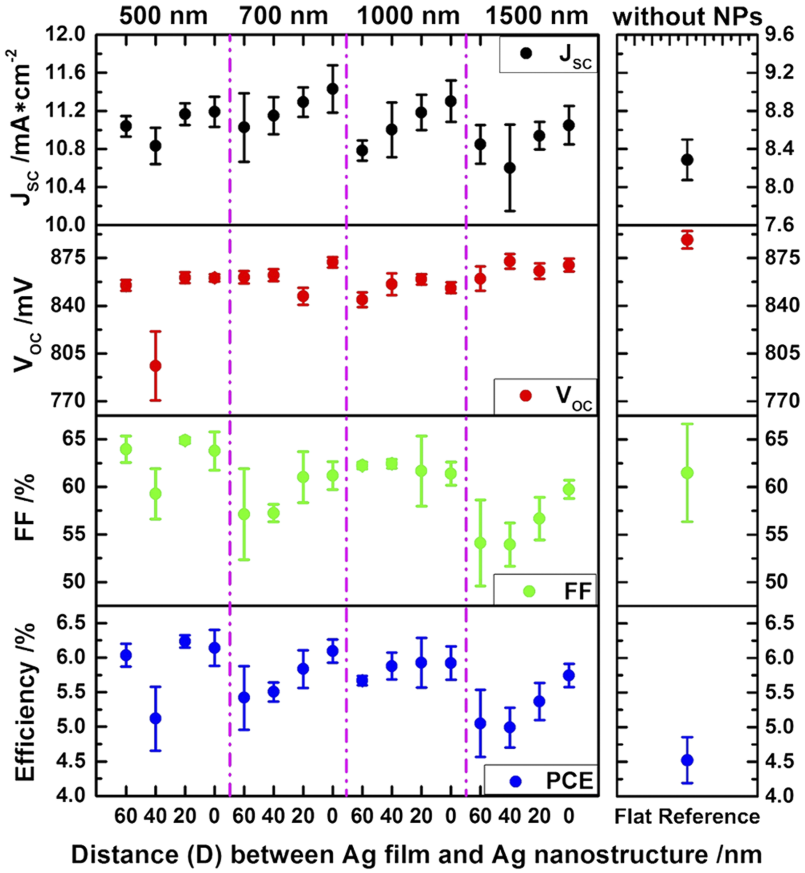

FIG. 3. Experimentally measured a-Si:H solar cell parameters for various distanced-values (Fig. 1 schematic) and periodicities (500, 700, 1000 and 1500 nm as indicated on the top). A total of 144 cells were measured, and each point is an average of 9 cells. The results for the flat reference (without NPs) cells are summarized on the right side. Note that the J_{SC} for the flat reference scale is presented in a different scale.

comparison. The goal here was not to optimize the deposition receipt for maximum efficiency, but to investigate the effects of nanostructuring. In that sense, we required a stable efficiency baseline (control) and a good degree of reproducibility between devices. These were achieved by processing all cells in exactly the same batch. The level of variation (error bars) in Figure 3 (average of 9 cells for each data point) confirm that the observed changes between cell geometries (and the control) are statistically significant.

In a first approximation, the trapping efficiency can be directly correlated to the J_{SC} value, assuming that J_{SC} is directly proportional to the number of photons captured by the solar cell absorber layer. Fig. 3 indicates that the maximum J_{SC} (11.4 ± 0.3 mA/cm^2) of all cells was obtained for the BR composed of the 700 nm periodicity Ag NP with D = 0 nm. The overall trend in Fig. 3 is an increase in J_{SC} when D decreases from 60 nm to 0 nm for a given periodicity. The best nanostructured solar cell (700 nm periodicity with D = 0 nm) shows a significant average J_{SC} improvement (~3 mA/cm^2) compared to the (flat) reference cell without Ag NPs. The improvement of J_{SC} in nanostructured solar cells compared to corresponding flat references has been well explored in the literature.[10,14,21] To further investigate the effect of the position of the NPs in the BR (variation of thickness D, see Figure 1) on the light trapping properties, EQEs were measured for all nanostructured a-Si:H solar cells as well as the flat reference. Fig. 4 shows typical EQE curves for different periodicities at D = 0 nm. The observed EQE curve from the flat reference presents typical interference fringes after 500 nm due to Fabry-Perot (FP) resonances.[22,23] Compared to the flat reference sample, the a-Si:H solar cells modified with Ag NPs show a significant EQE increase in the 500 to 750 nm region. This enhancement in EQE is more significant for smaller periodicities (P=500, 700 and 1000 nm) than for

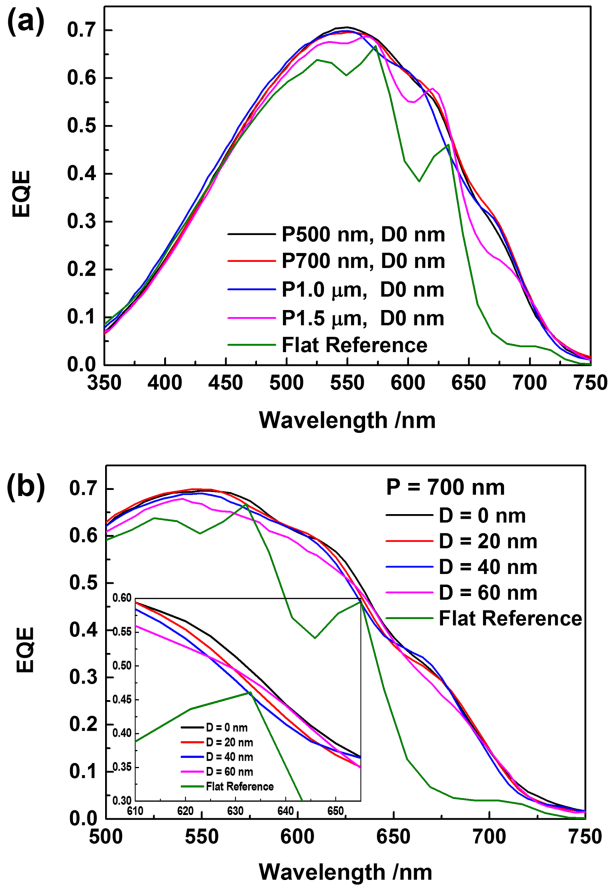

FIG. 4. (a) Ag NPs modified a-Si:H solar cells' EQE profile for different periodicities (indicated in the Fig.) and D = 0 nm. (b) Ag NPs modified a-Si:H solar cell with 700 nm periodicity for different D-values. A flat reference cell (without Ag NPs) is also included for comparison.

P=1.5 μm. The EQE profile for P=1.5 μm seems to be a mixture of the curves obtained from solar cells with NPs and the flat reference. The differences in the EQE among the solar cells with different periodicities (P=500, 700 and 1000 nm) are comparably small. The FP fringes in Fig. 4 vanish (Flat > P=1.5 μm > P=1 μm) with decreasing periodicity. Typical EQE curves describing the effect of the position of Ag NPs (D = 60, 40, 20 and 0 nm) on the solar cell BR are presented in Fig. 4b for a fixed NP periodicity of 700 nm (highest improvements compared to the flat reference). As it can be also deduced from Fig. 3, the current density is slightly higher for smaller values of D, where the NPs are furthest away from the silicon absorber.

These experimental observations may seem counterintuitive at a first glance, since the SPR electro-magnetic fields are highest at the Ag NPs surface from where they decay exponentially away from the metal. At D = 60 nm, the Ag NPs are closest to the solar cell absorber layer and would therefore contribute most to plasmonically induced current enhancements by field localization. In our experiments, the opposite trend was observed. Most improvements were found for the BR structure with the largest distance between absorber and NPs. From this result, one can deduce that near field enhancements might have only a minor influence on the solar cell performance for this configuration.

The J_{SC} dependence on periodicity and nanostructure geometry has been studied by many research groups.[4,22,24] In order to understand the effect of the NP position in this type of nanostructured a-Si:H solar cells, FDTD simulations were performed for the best cells: P = 700 nm (see SM for the simulation details). This approach allows a visualization of the light distribution inside the solar cell absorber layer, providing an insight into the correlation between the light-NP interactions with the enhanced photon absorption. Fig. 5a–d presents electric field intensity profiles inside the

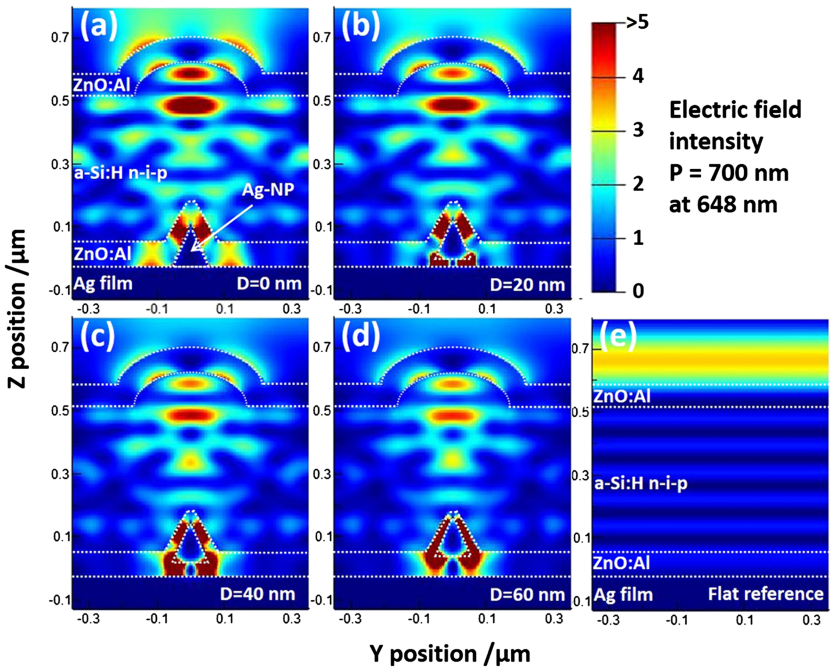

FIG. 5. FDTD simulations of electric field intensity profiles inside a Ag NPs modified a-Si:H solar cell for different Ag distance (D) relative to the BR contact (a-d). The cell configuration is indicated in the Fig. 1. (e) shows the flat reference cell without Ag NPs modification. The excitation wavelength is 648 nm and the periodicity is 700 nm in all graphs. The color scale is the same in all images (a-e). Electric field intensities > 5 (compared to the excitation light intensity) are shown in dark red color.

Ag NPs-modified a-Si:H solar cell for different D-values obtained from FDTD simulations at the Ag NPs SPR wavelength of 648nm. The simulation indicates that, in all cases, a strong near field confinement is mainly found in the ZnO:Al buffer layer adjacent to the Ag NP surface. At D = 60 nm (Fig. 5d), the enhanced electric field is almost totally confined inside the ZnO:Al layer at the Ag NP surface. Note that this enhanced near field SPR intensity is highest at the Ag NPs surface and decays evanescently into the doped silicon n-layer. The results from Figure 5 suggest that the position of the well-organized nanostructures can be used to minimize absorption in the doped a-Si:H layers (n and p). These regions exhibit high material defect densities, meaning that photons absorbed in these layers do not contribute to the photocurrent. This is confirmed by the calculated absorption in the i-layer of a-Si:H solar cells presented in Figure 6a. Notice that the nanostructure scatters the light back to the n-i-p region. However, electron-hole pairs formed in the i-layer are the dominant contribution to the photo-current. Therefore, the best position for the nanostructure will maximize light scattering towards the i-layer. When the Ag NPs distance from the silver BR increases from D = 0 nm to D = 60 nm (Fig. 6a), the absorption inside the a-Si:H absorber i-layer is significantly modified. As

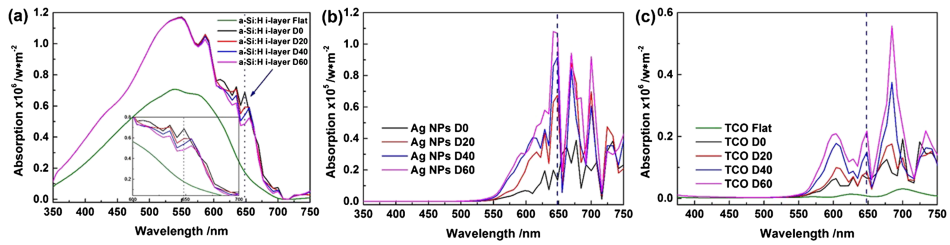

FIG. 6. FDTD calculated of absorption profiles of the Ag NPs modified (P = 700 nm) a-Si:H solar cells for different Ag distance (D as indicated) relative to the BR contact: (a) inside a-Si:H i-layer; (b) by Ag NPs nanostructures; (c) inside the ZnO:Al layers, respectively. The vertical dotted line indicated the 648 nm wavelength that is shown in Fig. 5 plots.

clearly seen in Fig. 5a–d, from the light distribution profile inside the a-Si:H solar cell, for D=0, the light is more confined inside the i-layer, where the built-in electric field leads to efficient separation of the photogenerated charge carriers. In addition, Fig. 6b quantitatively shows that for an increased distance D, an increased absorption by the Ag NPs is obtained for wavelengths between 550 nm to 750 nm due to SPR near field confinement. Fig. 6c also shows an increased absorption inside the ZnO:Al layer in the same spectral range with increasing distance D. As mentioned above, this implies that the SPR leads to an energy loss for the particular solar cell design presented here. We emphasize again that only electron-hole pairs generated inside the intrinsic a-Si:H layer are separated by the built-in electric field and contribute significantly to the current density. The light trapped (absorbed) elsewhere, quantified in Figure 6 (inside the doped layers (n and p layers), the ZnO:Al layer or the Ag NPs) leads to energy losses due to the recombination. Apart from the SPR effect, Fig. 5a–d show that the front dome-shaped nanostructure actually leads to an important focusing contribution. Figure 5a–d indicates that the electric field appears strongly confinement inside the absorber (a-Si:H) layer just below the front dome-shaped surface. As for the flat reference (Fig. 5e), the FP interference fringes dominate the light distribution inside the absorber layer. The field distributions in Figure 5 point towards a significant role played by the top (dome shaped) texture in keeping the light confined in the absorber layer. From both Fig. 5 and Fig. 6, it can be concluded that the best configuration is to place the Ag NPs at D = 0 nm. In this case, the combination of the back-scattering of the metal structure and the texturing on the top surface allows optimal light concentration in the i-layer of the absorber for these types of thin film solar cells. The computational result is in good agreement with the experimental J_{SC} trend shown in Fig. 3 and the experimental EQE results shown in Fig. 4b.

In this paper, the performance of Ag NPs modified a-Si:H solar cells was systematically studied. Both, experimental results and FDTD simulations suggest that the geometry of the cell structure and the position of the nanoparticles in the back contact have a higher influence on the light trapping properties than SPR field localization. In our experiments, the a-Si:H solar cells modified with Ag NPs, which were placed at the largest distance away from the absorber showed the highest improvement in J_{SC}, as this reduced the SPR-induced parasitic absorption both inside the TCO between the NPs and the Ag BR as well as inside the NP itself. FDTD simulations confirm that the front dome-shaped nanostructure actually shows an important focusing effect, Ag NPs located directly at the BR (D = 0 nm) yield the best light distribution inside the solar cell absorber layer (i-layer).

See supplementary material for the experimental details on the fabrication of the nanoparticle modified substrate, fabrication of solar cell, characterization, and FDTD simulation.

The authors gratefully thank Marion Luttmann, Tim Möller, and Alex Neumüller for cell development and depositions. Thank Adam Schuetze for FIB assistance and Walter Jaimes Salcedo for the simulation help. This work was supported by the Natural Sciences and Engineering Research Council (NSERC) of Canada, the Institute of Integrated Energy Systems at the University of Victoria (IESVic), UVic Center for Advanced Materials and Related Technologies (CAMTEC) and the DAAD financed graduate School "Science and Technology" OLTECH at the University of Oldenburg.

[1] Q. Zhang, E. Uchaker, S. L. Candelaria, and G. Cao, Chem. Soc. Rev. **42**(7), 3127 (2013); K. Yu and J. Chen, Nanoscale Research Letters **4**(1), 1 (2009); T. Gao, B. Wang, B. Ding, J.-kun Lee, and P. W. Leu, Nano Lett. **14**(4), 2105–2110 (2014); S.-F. Leung, L. Gu, Q. Zhang, K.-H. Tsui, J.-M. Shieh, C.-H. Shen, T.-H. Hsiao, C.-H. Hsu, L. Lu, D. Li, Q. Lin, and Z. Fan, Sci. Rep. **4**, 4243 (2014).
[2] Q. Lin, B. Hua, S.-fung Leung, X. Duan, and Z. Fan, ACS Nano **7**(3), 2725 (2013).
[3] C. Eminian, F. J. Haug, O. Cubero, X. Niquille, and C. Ballif, Progress in Photovoltaics: Research and Applications **19**(3), 260 (2011).
[4] U. W. Paetzold, E. Moulin, B. E. Pieters, R. Carius, and U. Rau, Opt. Express **19**(S6), A1219 (2011).
[5] V. E. Ferry, A. Polman, and H. A. Atwater, ACS Nano **5**(12), 10055 (2011).
[6] H.-P. Wang, T.-Y. Lin, M.-L. Tsai, W.-C. Tu, M.-Y. Huang, C.-W. Liu, Yu-L. Chueh, and Jr-H. He, ACS Nano **8**(3), 2959 (2014).
[7] K. N. Vijay and Y. Cui, Nanophotonics **2**(3), 187 (2013).
[8] H. A. Atwater and A. Polman, Nat Mater **9**(3), 205 (2010).
[9] H.-P. Wang, D.-H. Lien, M.-L. Tsai, C.-A. Lin, H.-C. Chang, K.-Y. Lai, and Jr-H. He, Journal of Materials Chemistry C **2**(17), 3144 (2014).
[10] P. Spinelli, V. E. Ferry, J. van de Groep, M. van Lare, M. A. Verschuuren, R. E. I. Schropp, H. A. Atwater, and A. Polman, Journal of Optics **14**(2), 024002 (2012).
[11] V. E. Ferry, J. N. Munday, and H. A. Atwater, Adv. Mater. **22**(43), 4794 (2010).

[12] M. Theuring, P. Hui Wang, M. Vehse, V. Steenhoff, K. von Maydell, C. Agert, and A. G. Brolo, J. Phys. Chem. lett. **5**(19), 3302 (2014).
[13] J. Niesen, B. P. Rand, P. Van Dorpe, D. Cheyns, L. Tong, A. Dmitriev, and P. Heremans, Advanced Energy Materials **3**(2), 145 (2013).
[14] K. Jung, H.-J. Song, G. Lee, Y. Ko, K. J. Ahn, H. Choi, J. Y. Kim, K. Ha, J. Song, J.-K. Lee, C. Lee, and M. Choi, ACS Nano **8**(3), 2590 (2014).
[15] T. S. Luk, N. T. Fofang, J. L. Cruz-Campa, I. Frank, and S. Campione, Opt. Express **22**(S5), A1372 (2014).
[16] H. Tan, R. Santbergen, A. H. M. Smets, and M. Zeman, Nano Lett. **12**(8), 4070 (2012).
[17] V. E. Ferry, M. A. Verschuuren, M. Claire van Lare, R. E. I. Schropp, H. A. Atwater, and A. Polman, Nano Lett. **11**(10), 4239 (2011); U. W. Paetzold, E. Moulin, D. Michaelis, W. Böttler, C. Wächter, V. Hagemann, M. Meier, R. Carius, and U. Rau, Appl. Phys. Lett. **99**(18), 181105 (2011).
[18] E. Moulin, J. Sukmanowski, M. Schulte, A. Gordijn, F. X. Royer, and H. Stiebig, Thin Solid Films **516**(20), 6813 (2008); E. Moulin, J. Sukmanowski, P. Luo, R. Carius, F. X. Royer, and H. Stiebig, J. Non·Cryst. Solids **354**(19–25), 2488 (2008).
[19] J. Bhattacharya, N. Chakravarty, S. Pattnaik, W. D. Slafer, R. Biswas, and V. L. Dalal, Appl. Phys. Lett. **99**(13), 131114 (2011); V. E. Ferry, M. A. Verschuuren, H. B. T. Li, E. Verhagen, R. J. Walters, R. E. I. Schropp, H. A. Atwater, and A. Polman, Opt. Express **18**(S2), A237 (2010); V. E. Ferry, M. A. Verschuuren, H. B. T. Li, R. E. I. Schropp, H. A. Atwater, and A. Polman, Appl. Phys. Lett. **95**(18), 183503 (2009).
[20] P. Colson, C. Henrist, and R. Cloots, Journal of Nanomaterials **2013**, 19 (2013); W. Y. Fu and H. W. Choi, "Nanosphere lithography for nitride semiconductors" (2010); X. L. Huang, D. Ratchford, P. E. Pehrsson, and J. Yeom, Nanotechnology **27**(39) (2016); J. Yu, C. Geng, L. Zheng, Z. Ma, T. Tan, X. Wang, Q. Yan, and D. Shen, Langmuir **28**(34), 12681 (2012).
[21] H. Huang, L. Lu, J. Wang, J. Yang, S.-F. Leung, Y. Wang, D. Chen, X. Chen, G. Shen, D. Li, and Z. Fan, Energy Environ. Sci. **6**(10), 2965 (2013); M. van Lare, F. Lenzmann, and A. Polman, Opt. Express **21**(18), 20738 (2013); M. G. Deceglie, V. E. Ferry, A. P. Alivisatos, and H. A. Atwater, Nano Lett. **12**(6), 2894 (2012).
[22] A. Micco, A. Ricciardi, M. Pisco, V. La Ferrara, L. V. Mercaldo, P. D. Veneri, A. Cutolo, and A. Cusano, J. Appl. Phys. **114**(6), 063103 (2013).
[23] I. Massiot, C. Colin, C. Sauvan, P. Lalanne, P. R. i Cabarrocas, J.-L. Pelouard, and S. Collin, Opt. Express **21**(S3), A372 (2013); X. H. Li, P. C. Li, D. Z. Hu, D. M. Schaadt, and E. T. Yu, J. Appl. Phys. **114**(4), 044310 (2013).
[24] T. K. Chong, J. Wilson, S. Mokkapati, and K. R. Catchpole, Journal of Optics **14**(2), 024012 (2012); S. Mokkapati and K. R. Catchpole, J. Appl. Phys. **112**(10), 101101 (2012).